Nanometer-level repeatable metrology using the Nanoruler

Paul T. Konkola,[a] Carl G. Chen, Ralf K. Heilmann, Chulmin Joo, Juan C. Montoya, Chih-Hao Chang, and Mark L. Schattenburg
Massachusetts Institute of Technology, Cambridge, Massachusetts 02139

(Received 26 June 2003; accepted 21 July 2003; published 10 December 2003)

We report on the measurement of the fringe-to-substrate phase error in our Nanoruler system. This system utilizes scanning beam interference lithography to pattern and measure large-area, nanometer-accuracy gratings that are appropriate for semiconductor and integrated opto-electronic metrology. We present the Nanonruler's metrology system that is based on digital frequency synthesizers, acousto-optics, and heterodyne phase sensing. It is used to assess the fringe-to-substrate placement stability and the accuracy of the feedback signals. The metrology system can perform measurements in real time, on the fly, and at arbitrary locations on the substrate. Experimental measurements are presented that demonstrate the nanometer-level repeatability of the system. Dominant error sources are highlighted. © *2003 American Vacuum Society.*
[DOI: 10.1116/1.1610003]

I. INTRODUCTION

Grating-based metrology[1] is an attractive solution for the measurement of patterning, replication, and process distortions. However, large gratings that can serve as placement references suitable for semiconductor metrology do not exist with the necessary nanometer-level accuracy.[2]

We are developing scanning beam interference lithography (SBIL) to pattern gratings and grids with nanometer-level accuracy. The system uses a scanned interference image to pattern large gratings—up to 300 mm in diameter. Figure 1 shows the front of the system where some of the major subassemblies are visible. This experimental system,[3,4] the "Nanoruler," employs interference lithography optics,[5] an *X-Y* air bearing stage, column referencing displacement interferometry, refractometry, a grating length-scale reference, a beam alignment system,[6] and acousto-optic fringe locking.[7] Supporting systems also include an environmental enclosure, a beam steering system,[8] and vibration isolation with feedforward.

The system design[3] is the result of considering the many error sources in the system. The major sources of errors include: thermal expansion, air index nonuniformity, periodic errors, electronic noise, vibration, substrate clamping, and control. The metrology system discussed in this article enhances the understanding of ultraprecision patterning in our system.

II. METROLOGY SYSTEM

The metrology interferometer system shown in Fig. 2 is based on digital frequency synthesizers, acousto-optics, and heterodyne phase sensing. This "reading mode" configuration is used to assess the fringe-to-grating motion and the unobservable errors in the system. While heterodyne sensing of grating phase has been done by other researchers,[9] the fringe locking and metrology system used in the Nanoruler is the first heterodyne system suitable for interference lithography where the fringe phase needs to be controlled. Furthermore, the design meets the associated requirements for patterning and metrology. The reading mode of the system, as opposed to the writing mode, is the focus of this article. Here the nominal frequencies to acousto-optic modulators AOM1 and AOM2 are 110 and 90 MHz, respectively. The frequency choice produces a heterodyne frequency of 20 MHz on the phase meters. The average offset of 100 MHz is chosen because the diffraction efficiency for our AOMs is highest in the 100 MHz range and a wide separation of zero and first order is achieved. The measurement of the fringe-to-grating motion is calculated from the PM_4 (phase meter 4) signal and is given by

$$x_4 = \frac{PM_4 \Lambda}{p}, \tag{1}$$

where PM_4 is the digital phase meter reading of the optical interference signal that is produced by the reflected zero order beam and the diffracted minus-one order beam. The variable Λ is the grating period and p is the integer number of phase meter counts per period. Since the beams are combined at the grating interface, the signal is a very accurate measurement of the fringe-to-grating motion, which occurs at that interface. Electronic errors are essentially the only source of inaccuracy for this measurement. The optical paths in reading and writing mode, for practical purposes, are identical. Therefore the stability and repeatability assessed by reading gratings is an accurate estimate of the fringe placement stability and repeatability when writing gratings.

The relative phase measurement between the right and left arms of the interferometer with respect to the fringe locking optics is the signal PM_3. The beam splitters for the phase sensing optics are located on a rigid and thermally stable "metrology block." The metrology block interferometer phase, in distance units, is given by

$$x_m = -\frac{PM_3 \Lambda}{p}, \tag{2}$$

[a]Electronic mail: konkola@mit.edu

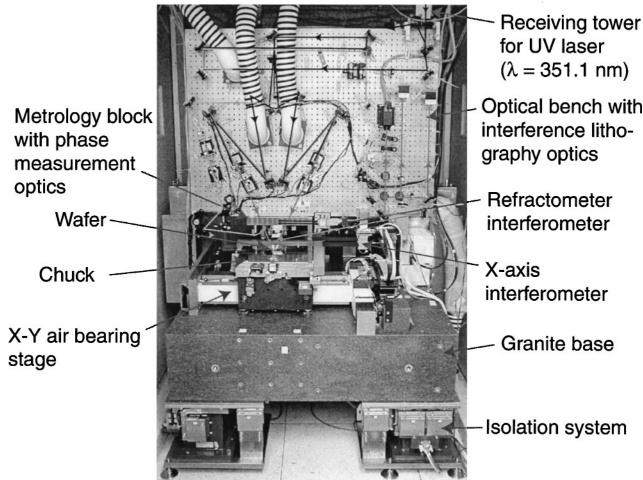

FIG. 1. Front of the Nanoruler showing major subassemblies.

which is the stability of the interference fringes relative to the metrology block optics. This metrology block interferometer phase is combined with the stage error signal to control the fringes. The fringe locking error signal, using distance units in the writing plane, is

$$x_{\mathrm{fle}} = x_m - x_{\mathrm{die}}. \tag{3}$$

This is the error signal that the fringe locking controls toward zero by shifting the AOM1 frequency f_1. The displacement interferometer error perpendicular to the fringes is x_{die}.

The fringe locking controller can operate in both reading and writing modes. Locking the fringes in reading mode allows the fringe-to-substrate displacement to be assessed under conditions that very closely approximate the writing mode condition. The fringe-to-substrate motion contains both the fringe locking error and the unobservable error. The unobservable error is obtained by removing any residual fringe locking error from x_4 and is given by

$$x_{\mathrm{ue}} = x_4 + x_{\mathrm{fle}}. \tag{4}$$

The unobservable error is the inaccuracy in the signals used to control the fringes. The unobservable error currently limits the placement stability in our system.

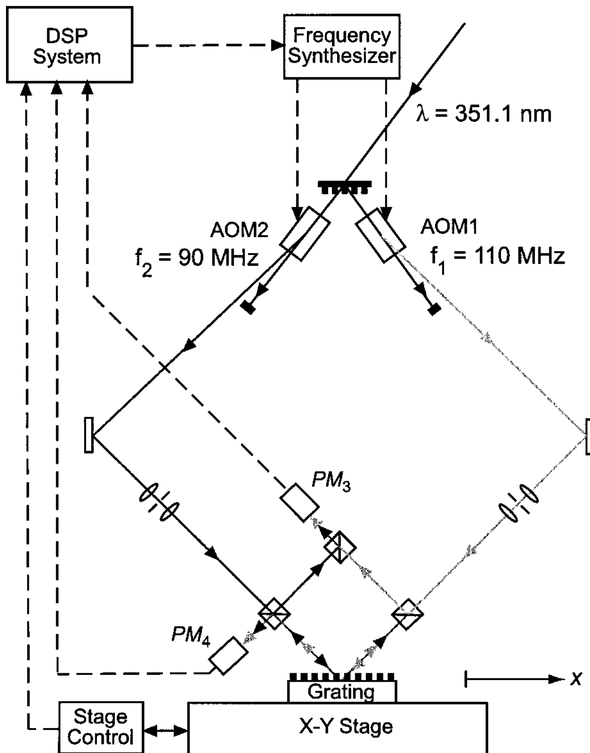

FIG. 2. System reading mode topology.

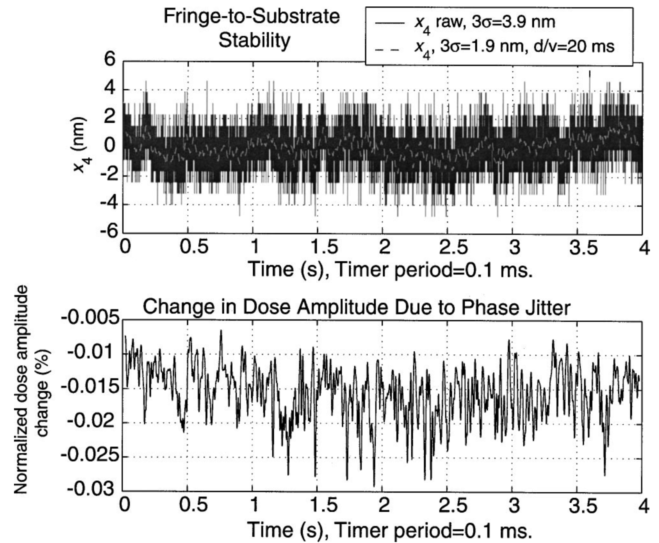

FIG. 3. Upper plot is the fringe-to-grating stability, x_4. The raw data sampled at 10 kHz and the estimated dose phase error is shown. The lower figure plots the calculated normalized dose amplitude change due to x_4 assuming $d/v = 20$ ms.

III. METROLOGY RESULTS

The fringe-to-substrate placement is the fundamental performance metric for SBIL. The upper plot of Fig. 3 shows x_4 over 4 s sampled at 10 kHz. The raw data is taken directly from the Zygo ZMI 2002 phase meters that were programmed to have an internal low pass filter with a −3 dB bandwidth of 15 kHz. The raw 3σ error in x_4 is 3.9 nm. The Gaussian filtered data is the dose phase error, which accounts for the integration of the intensity during the scanned exposure.[3] The Gaussian filtered data uses the d/v parameter of 20 ms, which, for instance, corresponds to a beam diameter of $d = 2$ mm and a stage velocity of $v = 100$ mm/s. The 3σ error for the Gaussian filtered data is 1.9 nm.

The exposure dose can be approximated as a dc background dose plus a sinusoidal dose.[3] The reduction in the amplitude of the sinusoidal dose component due to the phase jitter is plotted in the lower portion of Fig. 3. The normalized dose amplitude reduction is better than 0.03%. Thus the fringe jitter is small enough to provide excellent contrast. In the x_4 data, most of the residual fringe locking error is averaged by the Gaussian filter; the unobservable error at the same time is very nearly the same as x_4 for the Gaussian

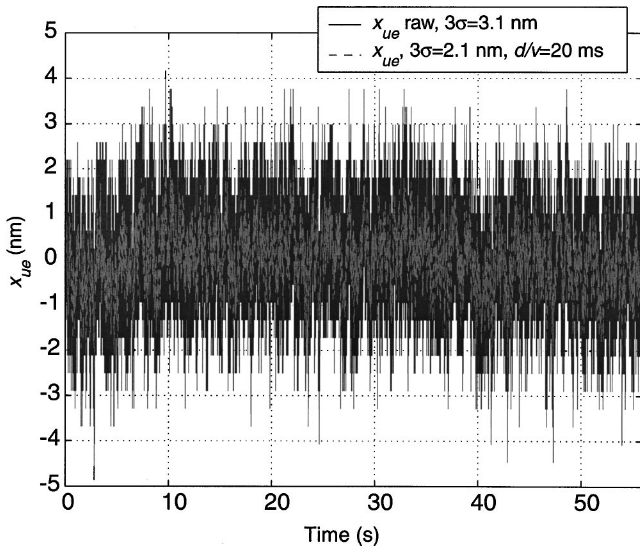

FIG. 4. Unobservable error x_{ue} over 56 s while the stage is static. Raw data bandlimited to 714 Hz and Gaussian filtered data are shown.

filtered data. The Gaussian filtered x_{ue} and x_4 errors are both 1.9 nm, 3σ. The unfiltered x_{ue} is notably better than x_4 with a 3σ of 3.1 nm.

Figure 4 shows x_{ue} over 56 s. The data was downsampled seven times from 10 kHz sampled data and it was filtered with a 714 Hz cutoff frequency to produce band limited data. The raw x_{ue} data has a 3σ variation of 3.1 nm and about 2.1 nm, 3σ for the Gaussian filtered data.

The (square root) power spectrum of the x_{ue} data from Fig. 4 is shown in Fig. 5. Distinctive error regions are noted in the figure. The fast cutoff in the Gaussian filtered data is evident. The significant errors at high frequency that are strongly filtered include those due to vibrations and most of the electrical noise. Even the 60 Hz electrical noise is filtered

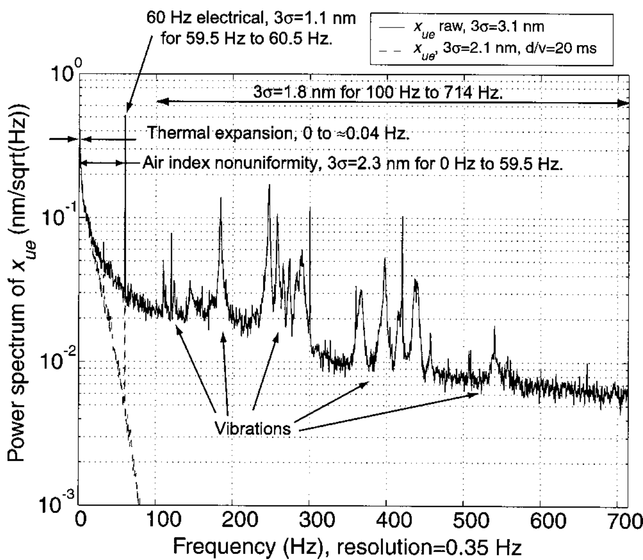

FIG. 5. Power spectrum of x_{ue} computed from the data in Fig. 4. The Gaussian filtered data shows the very fast cutoff. Dominant error sources in different frequency bands are indicated.

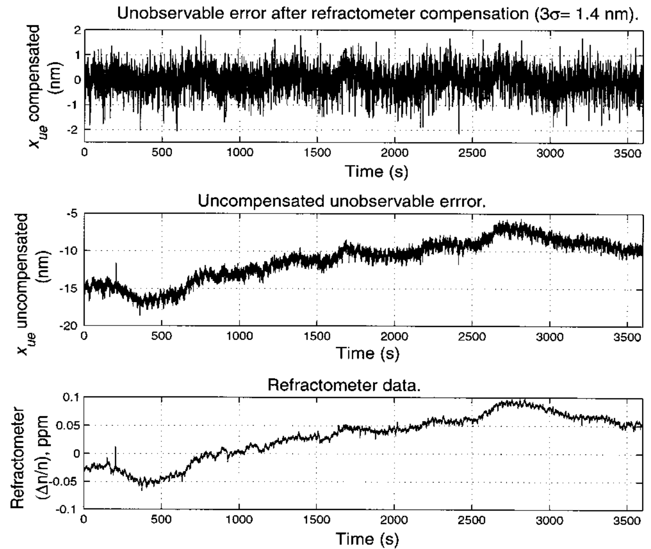

FIG. 6. Top plot is the long term unobservable error with refractometer compensation. The middle plot is the unobservable error without refractometer compensation. The bottom plot is the refractometer data taken at the same time. The data is bandlimited to 1.4 Hz.

by a factor of 6× when $d/v=20$ ms. The 3σ values shown in the figure were computed by integrating the power spectrum of the raw data. The air index nonuniformity and the part expansion errors, which occur at low frequencies, limit the performance of the system. Between 0 and 59.5 Hz the unobservable error is 2.3 nm, 3σ. The periodic error of the interferometers is also included in the low frequency errors. The periodic errors were separately assessed[3] to be 1.0 nm, 3σ and therefore they are not the dominant error source at this time.

The top plot of Fig. 6 shows the unobservable error over an hour. The long term stability is 1.4 nm, 3σ for this data that is bandlimited to 1.4 Hz. The refractometer signal shown in the lower plot was used as a correction. Over the hour the refractivity varied by 0.15 ppm, which leads to about 10 nm of error for the uncompensated data in the middle plot. Most of this refractivity variation is due to pressure changes.

The refractometer is not effective for compensating nonuniform index variations, which especially includes fluctuations faster than about 0.04 Hz as indicated in Fig. 7. The plot shows the (square root) power spectrum of the data from Fig. 6 for the compensated and uncompensated unobservable error as well as the refractometer correction. After 0.04 Hz the refractometer signal drops off much faster than the x_{ue} signals and the compensated data is no longer better than the uncompensated data. The larger x_{ue} at high frequency is expected since the velocity of the air in the refractometer beam path is believed to be much slower than the air velocity in the stage beam paths. Most of the error in the compensated data is attributed to the air index nonuniformity since much of the noise occurs over tens-of-seconds-long time scales or faster. Between 0.04 and 1.4 Hz, the 3σ square root power is 1.3 nm. Below 0.04 Hz, where the integrated error is 0.7 nm 3σ, thermal expansion is expected to dominate.

Considering the index sensitivity to temperature[10]

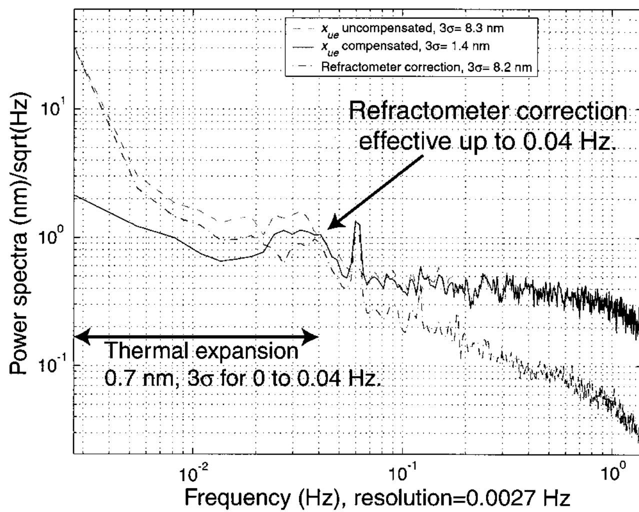

FIG. 7. Power spectra of the compensated and uncompensated x_{ue} data from Fig. 6. The power spectrum of the refractometer correction signal is also shown. The refractometer compensation is effective up to about 0.04 Hz.

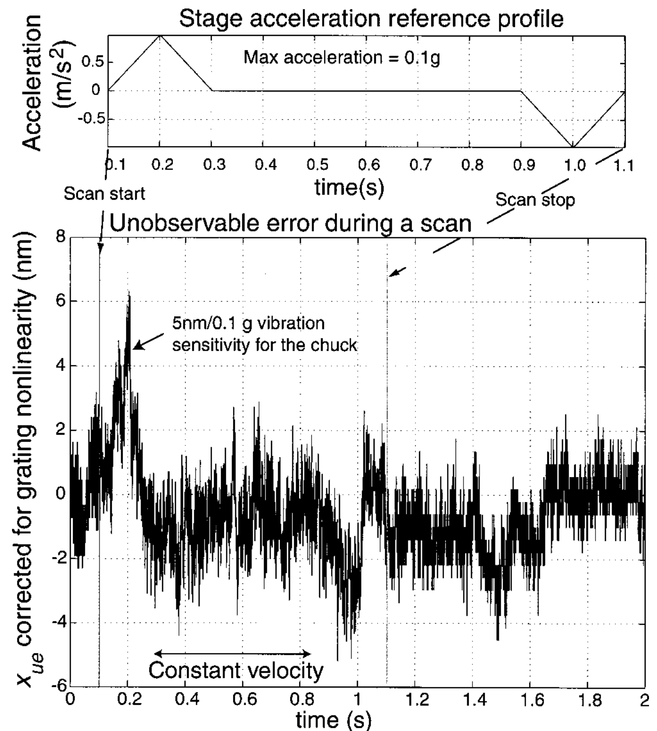

FIG. 8. Top plot shows the acceleration profile during a scan. This 8 cm long scan reaches 0.1 G peak acceleration and 0.1 m/s peak velocity. The bottom plot shows the unobservable error during the scan. During the times when the stage is moving at constant velocity and after it stops moving there is no noticeable increase in the unobservable error over the static case.

(dn/dT) of -0.9 ppb/mK, the total air index nonuniformity might be entirely explained by the temperature nonuniformity. The demonstrated temperature stability in our system is ± 7 mK using thermistors with 10 s time constants. Over shorter time scales, significant additional instability is expected. Also, temperature gradients up to 15 mK per 0.3 m have been measured.

When the stage is scanning, disturbances in addition to the static ones are present—the static and dynamic disturbances linearly superpose. Dynamic errors occur because of stage accelerations. The stage must accelerate to reach a constant velocity and the stage accelerates in response to disturbance forces, which increase during scanning. Additional stage errors occur in both the scan direction and in the perpendicular scan direction. Errors result because the chuck distorts under its own inertial forces and the metrology block optics displace during payload accelerations. Most of the reaction forces that disturb the payload are compensated by feedforward to the isolation system motors but they are never completely canceled. The unobservable errors due to vibration and deflections will be direct errors. The observable errors can be corrected by the fringe locking controller. At some point, the finite disturbance rejection of the controller is also an issue.

The lower plot of Fig. 8 shows x_{ue} during an 8 cm long stage scan with 100 mm/s peak velocity and 0.1 G peak acceleration. The vertical lines denote the start and stop of the stage profile motion. The stage acceleration profile for the moving portion is shown in the upper plot of Fig. 8. The unobservable error shows noticeable response during the stage accelerations but no obviously worse performance during the constant velocity portion of the scan or after the stage stops. The data while the stage is moving is corrected for any nonlinearity in the grating itself by applying data from a much slower scan. Because the SBIL system exposes the substrate during the constant velocity portion of the scan, the additional x_{ue} during acceleration is not a concern. This additional error during the acceleration is mainly due to deflections of the chuck and possibly the Abbe offset error associated with the stage yaw. The measured sensitivity to stage y accelerations is 5 nm per 0.1 G.

In a separate analysis,[3] the vibration errors of the system are assessed to be less than 1 Å. The smooth stage control, feedforward of the stage reaction forces to isolation system motors, and very rigid metrology frames were important factors in achieving this performance.

The grating phase across the entire wafer can be mapped via SBIL. The wafer mapping capability makes the Nanoruler a placement metrology tool in addition to a grating pattering tool. The repeatability of the wafer mapping is plotted in Fig. 9. This data is the difference between two wafer maps taken with a stage scan speed of 1 cm/s, while low pass filtering with a cutoff frequency of 8.7 Hz. The tool takes about 10 min to map a 100 mm wafer at this speed. The repeatability is 2.9 nm, 3σ. The wafer was not removed from the chuck between maps. Since integrating the power spectrum for x_{ue} in Fig. 5 from 0 to 8.7 Hz produces a 3σ error of 1.9 nm and subtracting two data sets should account for a $\sqrt{2}$ greater error, the 3σ error of 2.7 nm was expected by just considering the static data. Because the mapping requires stage motion, the associated thermal gradients and larger deadpath are expected to cause the slightly larger mapping error. The average period was measured to be consistent to 6 ppb and the rotation angle of the wafer was consistent to 1 nrad between maps.

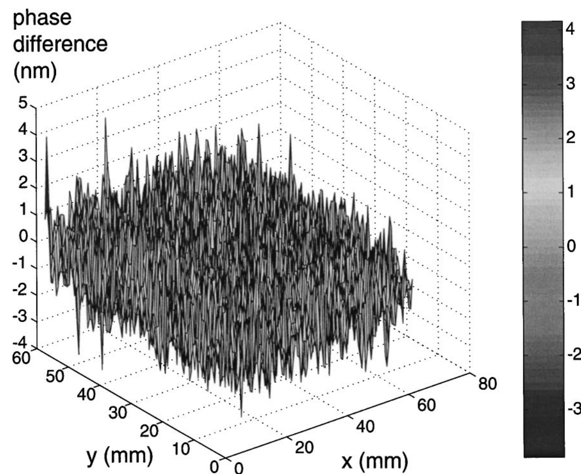

FIG. 9. Wafer phase mapping repeatability (nm). The 3σ repeatability for mapping an unrechucked wafer is 2.9 nm.

IV. CONCLUSIONS

We measured the short and long term errors of the system. Errors during scanning and errors during wafer mapping routines were also presented. We demonstrated long term (1 h) fringe placement stability of 1.4 nm, 3σ (0–1.4 Hz). Also, the short term placement stability is less than 4 nm, 3σ (0–5 kHz). When considering the integrated intensity of the scanned image traveling at 100 mm/s, the dose placement stability is 2.1 nm, 3σ. Dynamic errors due to scanning at 100 mm/s are negligible. The wafer mapping repeatability was shown to be 2.9 nm, 3σ while measuring a 100 mm substrate.

The errors in the system are presently limited by the air index nonuniformity. Future improvements might include compacting the fringe locking optics and enclosing the x-axis interferometer in a sliding vacuum containment.

The repeatability demonstrated in this article marks major progress toward nanometer accurate gratings. Future work needs to apply the Nanoruler's wafer mapping capability and self-calibration techniques[11–13] to achieve nanometer-level accuracy.

ACKNOWLEDGMENTS

The authors gratefully acknowledge the outstanding technical assistance of Robert Fleming and Edward Murphy. Student, staff, and facility support from the Space Nanotechnology Laboratory and the NanoStructures Laboratory at MIT are also appreciated. This work was supported by DARPA under Grant No. DAAG55-98-1-0130 and NASA under Grant No. NAG5-5271.

[1] M. Schattenburg *et al.*, J. Vac. Sci. Technol. B **17**, 2638 (1999).
[2] *International Technology Roadmap for Semiconductors Update*, International Technology Roadmap for Semiconductors, http://public.itrs.net, 2002.
[3] P. T. Konkola, Ph.D. dissertation, Massachusetts Institute of Technology, Department of Mechanical Engineering, 2003.
[4] P. T. Konkola *et al.*, *Proceedings of the 16th Annual Meeting of the American Society of Precision Engineering* (American Society for Precision Engineering, Crystal City, Virginia, 2001).
[5] C. G. Chen, Ph.D. dissertation, Massachusetts Institute of Technology, Department of Electrical Engineering and Computer Science, 2003.
[6] C. G. Chen *et al.*, J. Vac. Sci. Technol. B **20**, 3071 (2002).
[7] R. K. Heilmann *et al.*, J. Vac. Sci. Technol. B **19**, 2342 (2001).
[8] P. T. Konkola, C. G. Chen, R. K. Heilmann, and M. L. Schattenburg, J. Vac. Sci. Technol. B **18**, 3282 (2000).
[9] M. Suzuki and A. Une, J. Vac. Sci. Technol. B **7**, 1971 (1989).
[10] K. P. Birch and M. J. Downs, Metrologia **31**, 315 (1994).
[11] C. J. Evans, R. J. Hocken, and W. T. Estler, CIRP Ann. **45**, 617 (1996).
[12] M. R. Raugh, J. Vac. Sci. Technol. B **15**, 2139 (1997).
[13] M. T. Takac *et al.*, J. Vac. Sci. Technol. B **15**, 2173 (1997).